

# The interplay between screening properties and colloid anisotropy: Towards a reliable pair potential for disc-like charged particles

R. Agra<sup>1</sup>, E. Trizac<sup>1,a</sup>, and L. Bocquet<sup>2</sup>

<sup>1</sup> Laboratoire de Physique Théorique, Université de Paris XI, Bâtiment 210, 91405 Orsay Cédex, France

<sup>2</sup> Laboratoire de Physique de la Matière Condensée et Nanostructures, Université Lyon 1, 69622 Villeurbanne, France

Received 20 July 2004 /

Published online: 29 November 2004 – © EDP Sciences / Società Italiana di Fisica / Springer-Verlag 2004

**Abstract.** The electrostatic potential of a highly charged disc (clay platelet) in an electrolyte is investigated in detail. The corresponding non-linear Poisson-Boltzmann (PB) equation is solved numerically, and we show that the far-field behaviour (relevant for colloidal interactions in dilute suspensions) is exactly that obtained within linearized PB theory, with the surface boundary condition of a uniform potential. The latter linear problem is solved by a new semi-analytical procedure and both the potential amplitude (quantified by an effective charge) and potential anisotropy coincide closely within PB and linearized PB, provided the disc bare charge is high enough. This anisotropy remains at all scales; it is encoded in a function that may vary over several orders of magnitude depending on the azimuthal angle under which the disc is seen. The results allow to construct a pair potential for discs interaction, that is strongly orientation dependent.

**PACS.** 82.70.-y Disperse systems; complex fluids – 82.70.Kj Emulsions and suspensions – 83.80.Kn Physical gels and microgels

## 1 Introduction

Clays, in the generic form of charged platelets, enjoy widespread use in applications ranging from drilling, rheology modification (for paints, cosmetics, cleansers ...), catalysis etc. As a significant component of soils, clays are also of importance for crop production. The difficulty of synthesizing clays with well-controlled properties (size, composition, charge ...) has long hindered their fundamental study. The situation has considerably changed in the last ten years, with the increasing availability of customized synthetic clays, among which Laponite is a prominent example. Yet, our understanding of such systems is rudimentary (see, *e.g.* [1–8] and references therein).

A reasonable model for Laponite platelets is that of uniformly charged and infinitely thin discs [9]. In this paper, the focus will be on electrostatic interactions between identical charged discs, a crucial ingredient for understanding the phase behaviour and stability of clays in suspensions. The high anisotropy of these objects makes analytical progress difficult. In addition, these discs are typically highly charged, and the electrostatic coupling with their electrolytic environment (microscopic charged species) needs to be described by non-linear theories: the

plain linear Debye-Hückel approach should fail. We will work here in the common framework of non-linear Poisson-Boltzmann (PB) theory, where the (dimensionless) electrostatic potential outside the charged macroions obeys an equation of the form  $\nabla^2\phi = \kappa^2 \sinh \phi$ , assuming for simplicity monovalent microions only, the density of which governs the screening length  $\kappa^{-1}$  (the Debye length).

In a solution, the typical distance between macroions is often larger than the Debye length (this condition requires a minimal but nevertheless small amount of salt). At these “large” scales, the potential created by a given disc is small enough —compared to thermal agitation— to allow for the linearization of the PB equation:  $\nabla^2\phi \simeq \kappa^2\phi$ . Accordingly, the potentials within non-linear PB on the one hand, and linearized PB theory with a *suitably chosen boundary condition* on the other hand, coincide at large enough distance from the colloids, be they of discotic or other shapes. An analytical treatment within linearized PB (LPB) is of course considerably simpler than within PB, but the above remark may be of little practical help if one is not able to derive the relevant boundary condition on the colloid (effective potential), such that the corresponding LPB solution reproduces the PB one in the region of low enough potential. Close to the colloids, non-linear effects prevail (LPB and PB solutions strongly differ), and broadly speaking, microions —essentially counterions—

<sup>a</sup> e-mail: trizac@ipno.in2p3.fr

suffer there a high electrostatic coupling and may be considered as “bound”. They decrease the bare charge of the colloid so that its electrostatic signature at large distance defines an effective charge which is usually smaller in absolute value than the bare one (close to the colloid, the effective potential is accordingly smaller in magnitude than its non-linear counterpart).

For a unique charged sphere in an infinite electrolyte (infinite dilution limit), PB and LPB theories give rise to the same far-field behaviour, of Yukawa type ( $\exp(-\kappa r)/r$ , where  $r$  is the radial coordinate); non-linear effects only affect the prefactor (from which the effective charge is defined), preserving the functional form of the potential; the same remark equally applies to an infinite rod [10–12] (see also [13]). The situation changes, however, for anisotropic objects such as discs or finite-size rods [14], where non-linear screening phenomena generically affect the functional form of the potential and cannot be subsumed in an effective charge only. In other words, whereas the symmetry of the effective colloid clearly remains spherical in the case of spheres, predicting the symmetry of the effective charge distribution and associated electrostatic potential for a highly charged disc is a non-trivial question.

It is the purpose of the present work to study how non-linear screening effects and anisotropy conspire to affect the far-field behaviour in the case of discs. It has been shown in [15] that highly charged spheres and infinite rods may be considered as objects of constant effective potential  $\phi_{\text{eff}}$  (in the sense that  $\phi_{\text{eff}}$  becomes independent of physico-chemical parameters, provided that  $\kappa a > 1$  where  $a$  is the colloid radius. The complementary results reported here indicate that the constant potential picture goes in fact beyond this analysis, and give the correct symmetry of the effective charge distribution onto the disc. Such a boundary condition (within LPB theory) produces the same electrostatic potential as a highly charged disc within PB. A physical argument allowing to anticipate this correspondence will be presented in Section 2. Since the exact LPB solution for a disc held at constant potential in an electrolyte is not known, we will introduce in Section 3 a semi-analytical procedure to solve this problem. The characteristic features of the electrostatic potential relevant for clay discs will be obtained, and in order to assess the validity of the constant potential picture, the corresponding electrostatic potential will be compared in Section 4 to the solutions of the full non-linear PB theory. The latter will be obtained through an iterative numerical procedure. From these results, a pair potential will be constructed for charged discs, that has the same status as the celebrated Derjaguin-Landau-Verwey-Overbeek expression relevant for spheres [10–12], and includes charge renormalization. Concluding remarks will finally be presented in Sections 5 and 6.

## 2 The constant effective potential picture: why?

A disc of radius  $a$  and uniform surface charge density  $\sigma_{\text{bare}} = Z_{\text{bare}} e/(\pi a^2)$  is immersed in an infinite sea of elec-

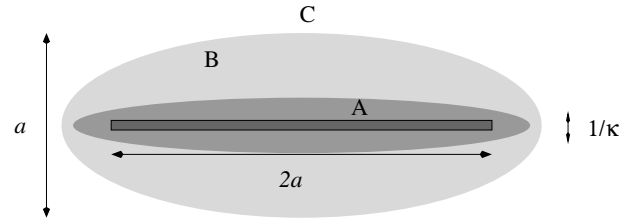


Fig. 1. Schematic side view of the charged platelet.

trolyte with bulk density  $n_s$ . From the permittivity  $\varepsilon$  of the solvent, the Bjerrum length is defined as  $\ell_B = e^2/(\varepsilon kT)$ , where  $kT$  is the thermal energy and  $e$  denotes the elementary charge. Within non-linear Poisson-Boltzmann theory, the dimensionless potential ( $\phi = e\varphi/(kT)$ ,  $\varphi$  being the original electrostatic potential) created by the disc obeys the following equation:

$$\nabla^2 \phi = \kappa^2 \sinh(\phi), \quad (1)$$

where  $\kappa$  is the inverse Debye length defined through  $\kappa^2 = 8\pi\ell_B n_s$ . For convenience,  $\phi$  is chosen to vanish at infinity. Equation (1) holds outside the disc.

Considering a highly charged disc with furthermore  $\kappa a > 1$ , one may partition space into three regions, as sketched in Figure 1. In region A, the electrostatic coupling between the colloidal disc and the microions is most important and one has  $\phi > 1$ . Outside A, in regions B and C, one has  $\phi < 1$  and PB equation (1) may be linearized; the corresponding Helmholtz-like LPB equation reads

$$\nabla^2 \phi = \kappa^2 \phi. \quad (2)$$

In addition, in region B,  $\phi$  is of unidimensional character and well approximated by the potential created by an infinite charged plane. *Ex contrario*, in region C,  $\phi$  regains its full 3D nature (2D here with the present azimuthal symmetry). The lateral extension of the “non-linear region” A is given by  $\kappa^{-1}$  while  $a$  measures the extension of region B. Since we assume  $\kappa a > 1$ , we have  $A \subset B$  and moving away from the disc, non-linear effects disappear before the finite size of the disc becomes relevant. In other words, B is the non-vanishing intersection between the “linear” region and its one-dimensional counterpart, where the solution of equation (1) takes the form [16]

$$\phi_{1D} = 4 \operatorname{arctanh}(\gamma e^{-\kappa z}) \quad (3)$$

$$\simeq 4\gamma e^{-\kappa z} \quad \text{in region B.} \quad (4)$$

In these expressions,  $z$  denotes the distance to the plane and, assuming without loss of generality a positive bare charge  $\sigma_{\text{bare}}$ ,  $\gamma$  is the positive root of the quadratic equation

$$\gamma^2 - \frac{\kappa e}{\pi \sigma_{\text{bare}} \ell_B} \gamma + 1 = 0. \quad (5)$$

In colloidal dispersions, the relevant range for the interactions is that of far field (except for dense systems) and the behaviour in the non-linear region (A) is of little interest.

From equation (4), it appears that the potential felt in the linear region B+C, when extrapolated to contact ( $z = 0$ ), reads  $\phi_{\text{eff}} = 4\gamma$ . As a consequence, solving LPB equation (2) with this boundary condition should provide the same potential outside region A as the PB solution of equation (1).

The above remarks follow from the constraint  $a > \kappa^{-1}$  and apply irrespective of the value of the bare charge. In particular,  $\sigma_{\text{bare}}$  (hence  $\phi_{\text{eff}}$  through  $\gamma$ ) may be position dependent on the disc. However, we are interested here in highly charged discs for which the non-linear region A exists (for low  $\sigma_{\text{bare}}$ , region A disappears; PB and LPB solutions coincide *at all distances* and the issue of effective potentials becomes trivial: effective and bare charges are equal). From equation (5), it appears that  $0 < \gamma < 1$  and that  $\gamma \rightarrow 1$  when  $\sigma_{\text{bare}}$  becomes large, so that  $\phi_{\text{eff}} \rightarrow 4$ , and the field created is independent of the bare charge. More details concerning the phenomenon of effective charge saturation may be found in [15].

We conclude here that a highly charged disc should effectively behave as a constant potential object treated within a linear theory. The corresponding LPB problem will be addressed in the following section but we emphasize before that the argument developed here provides  $\phi_{\text{eff}}$  to leading order in  $\kappa a$ . On the basis of the behaviour of charged spheres for which the curvature correction has been computed in [17] (leading to the result  $\phi_{\text{eff}} = 4 + 2/(1 + \kappa a) + \mathcal{O}(\kappa a)^{-2}$ ), we anticipate that  $\phi_{\text{eff}}$  may exceed the threshold 4. A similar behaviour is observed for cylinders of infinite length [17].

### 3 Semi-analytical solution of the Dirichlet linearized PB problem

#### 3.1 Methodology

If the solution of LPB equation (2) with Dirichlet boundary condition  $\phi = \phi_0$  was known analytically, the effective charge of highly charged discs [18] would follow immediately, enforcing  $\phi_0 = 4$  on the disc surface. Unfortunately, such a solution only exists in vacuum (*i.e.* when  $\kappa = 0$  [19]). To our knowledge, the only solution known at finite  $\kappa$  is that associated to Neumann boundary conditions (uniform surface charge) [20]. To solve the Dirichlet problem, we have therefore developed a semi-analytical procedure where the problem at hand is recast into a Fredholm integral equation (see below and App. A).

The general solution of equation (2) may be written assuming both cylindrical symmetry around an axis ( $Oz$ ), and reflection symmetry  $z \leftrightarrow -z$ :

$$\phi(\rho, z) = \int_0^\infty A(k) J_0(k\rho) e^{-\sqrt{k^2 + \kappa^2}|z|} dk. \quad (6)$$

In this relation,  $(\rho, z)$  denote the cylindrical coordinates and  $J_0$  is the Bessel function of order 0. The difficulty in the present situation is that the boundary conditions im-

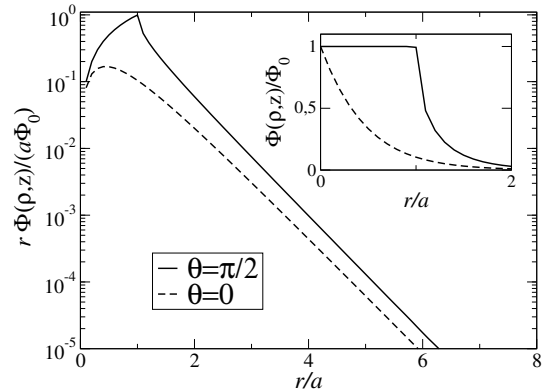


**Fig. 2.** Solution of LPB equation (2) with Dirichlet boundary condition of a uniform potential  $\phi = \phi_0$  on the disc surface. The quantity  $r\phi$  is shown on a linear-log scale to emphasize the far-field behaviour. Here,  $\kappa a = 2$  and  $r = \sqrt{\rho^2 + z^2}$  denotes the distance to the disc center. The continuous curve shows the potential in the direction  $\theta = \pi/2$  (as a function of  $r/a = \rho/a$ ), whereas the dashed line shows the behaviour as a function of  $r/a = z/a$  along normal axis  $\rho = 0$  ( $\theta = 0$ ). The inset shows  $\phi/\phi_0$  on a linear scale, again in the two perpendicular directions  $\theta = 0$  and  $\theta = \pi/2$ .

ply that the weight function  $A(k)$  obeys the mixed system

$$\int_0^\infty A(k) J_0(k\rho) dk = \phi_0, \quad \text{for } \rho < a, \quad (7)$$

$$\int_0^\infty \sqrt{k^2 + \kappa^2} A(k) J_0(k\rho) dk = 0, \quad \text{for } \rho > a, \quad (8)$$

where the second equation follows from the vanishing of the normal electric field  $\partial_z \phi$  on the symmetry plane  $z = 0$ . Starting from equations (7) and (8), the problem is rephrased in terms of an integral equation, solved numerically, from which the function  $A(k)$  is computed (see App. A). The potential then follows from (6).

#### 3.2 Properties of the solutions

A typical solution is shown in Figure 2. In the remainder, the variable  $\theta \in [0, \pi/2]$  denotes the angle between a given direction and the normal to the disc ( $\theta = \pi/2$  in the symmetry plane  $z = 0$  and  $\theta = 0$  along the normal to the disc, *i.e.* when  $\rho = 0$ ). It may be observed that the potential is anisotropic at all distances, a generic feature of screened electrostatics [4, 14]: the behaviours for  $\theta = 0$  and  $\theta = \pi/2$  strongly differ, at all scales. The anisotropy of the potential at large scales is encoded in a function  $f(\kappa a, \theta)$ , such that expression (6) may be written, for  $\kappa r \gg 1$ ,

$$\phi(r, \theta) \sim Z \ell_B f(\kappa a, \theta) \frac{e^{-\kappa r}}{r} + \mathcal{O}\left(\frac{e^{-\kappa r}}{r^2}\right), \quad (9)$$

where  $r = (\rho^2 + z^2)^{1/2}$  again denotes the distance to the disc center. In equation (9), the total charge  $Z$  of the

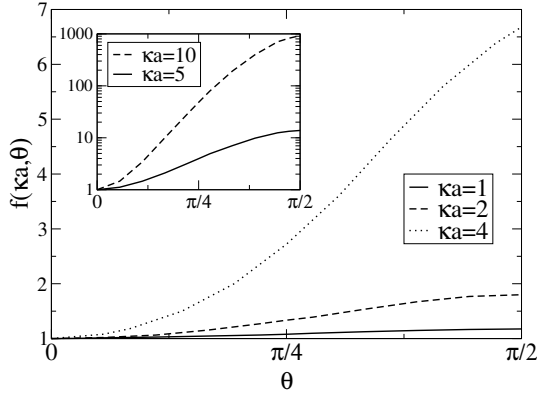


**Fig. 3.** Anisotropy function for  $\kappa a = 1, 2$  and  $4$  as a function of the azimuthal angle. The inset shows the results on a linear-log scale, for  $\kappa a = 5$  and  $\kappa a = 10$ .

platelet appears.  $Z$  is the integral over the disc surface of the surface charge density  $\sigma(\rho)$  [ $Ze = \int_{\text{disc}} \sigma(\mathbf{s}) d^2\mathbf{s}$ ]. This density turns out to be related to the anisotropy function through

$$f(\kappa a, \theta) = \int_{\text{disc}} \frac{\sigma(\mathbf{s})}{Ze} \exp(-\kappa \hat{\mathbf{r}} \cdot \mathbf{s}) d^2\mathbf{s}, \quad (10)$$

$\hat{\mathbf{r}}$  being a unit vector pointing in the  $\theta$ -direction. As expected, without electrolyte,  $\kappa$  vanishes so that  $f = 1$  and the potential in (9) takes the familiar form of an isotropic unscreened Coulomb expression.

The anisotropy function  $f$  and the total charge  $Z$ , are the key quantities governing far-field behaviour. Note that  $Z$  is not known *a priori* since only the surface potential is imposed. It may be shown that  $f$  is related to the weight function  $A(k)$  appearing in (6) through

$$\frac{Ze}{\epsilon} f(\kappa a, \theta) = -i \frac{A(i\kappa \sin \theta)}{\tan \theta}. \quad (11)$$

For small arguments, one has  $A(x) \propto x$  so that  $f(\kappa a, 0) = 1$ , which also means that the total charge is directly accessible through the behaviour along the  $\theta = 0$  axis:

$$\phi(r, 0) \sim Z \ell_B \frac{e^{-\kappa r}}{r}. \quad (12)$$

Note also that  $f(\kappa a, 0) = 1$  directly follows from (10) since  $\hat{\mathbf{r}} \cdot \mathbf{s} = 0$  when  $\theta = 0$ .

Figure 3 shows  $f(\kappa a, \theta)$  for different salinity conditions. This function increases with  $\theta$  and may take large values when  $\kappa a$  exceeds a few units (see the inset where the  $y$ -axis is shown in log scale). On the other hand, for  $\kappa a < 1$ ,  $f$  remains close to unity in all directions. The potential is strongest in the disc plane ( $\theta = \pi/2$ ), and increasing screening ( $\kappa$ ), one also strongly increases the anisotropy of the electrostatic potential. For a reasonable value  $\kappa a = 10$ ,  $f(\theta)$  varies by almost 3 orders of magnitude (a factor 930). In Figure 4, the complementary information concerning the total charge  $Z$  is displayed. This quantity

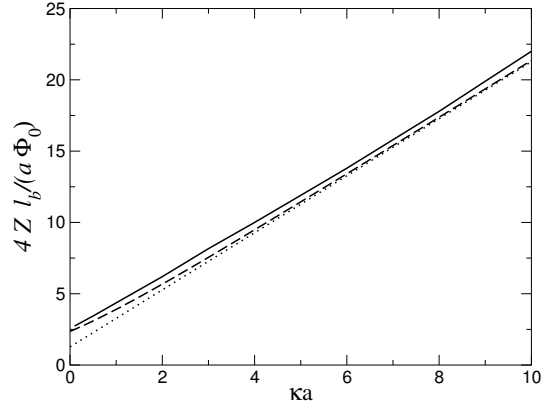


**Fig. 4.** Charge  $4Z\ell_B/(a\phi_0)$  as a function of  $\kappa a$  (continuous curve). The dashed line shows the result obtained within the simplified two-parameter model (Eqs. (15) and (17-18), see text). The dotted line corresponds to equation (20).

will be further discussed in Section 3.3. Note that  $f(\kappa a, \theta)$  does not depend on  $\phi_0$ , since it probes the repartition of surface charge distribution, not its overall magnitude. On the other hand,  $Z$  scales linearly with  $\phi_0$ .

### 3.3 An approximate expression for the anisotropy function and charge

It is instructive and useful for practical purposes to have an approximate analytical expression for the function  $f(\kappa a, \theta)$ . From equation (10), that may be rewritten

$$f(\kappa a, \theta) = \frac{2\pi}{Ze} \int_0^a I_0(\kappa \rho \sin \theta) \sigma(\rho) \rho d\rho, \quad (13)$$

this amounts to look for an approximate expression for the surface charge density  $\sigma$ . To this aim, we recall [21] that for an ideal conducting disc when  $\kappa = 0$ ,  $\sigma$  diverges in the vicinity of the edge ( $\rho \rightarrow a$ ), since

$$\sigma(\rho) = \frac{e\phi_0}{2\pi^2 a \ell_B} \frac{1}{\sqrt{1 - (\rho/a)^2}}. \quad (14)$$

Recall that  $\phi_0$  denotes the dimensionless electrostatic potential  $\phi = \varphi/(\epsilon kT)$ . The singularity of the electric field near sharp edges, which is the reason for the efficiency of lightning conductors, also pertains in presence of an electrolyte. We indeed show in Appendix B that when  $\kappa \neq 0$ , the Dirichlet solution to equation (2) exhibits a similar divergence as that present in equation (14), namely  $\sigma \propto (a - \rho)^{-1/2}$ .

A very simple two-parameter ansatz fulfilling this divergence requirement is

$$\sigma(\rho) = \sigma_0 + \sigma_1 \frac{1}{2\sqrt{1 - (\rho/a)^2}}. \quad (15)$$

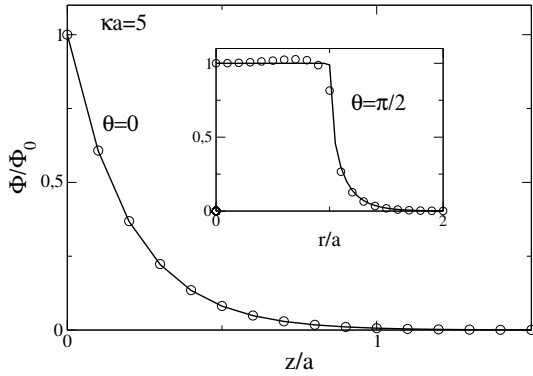


**Fig. 5.** Electrostatic potential following from the two-parameter approximation (circles) compared to the exact result (continuous curve, obtained following the method detailed in Sect. 3.1 and App. A). The main graph corresponds to  $\theta = 0$  and the inset to  $\theta = \pi/2$ .

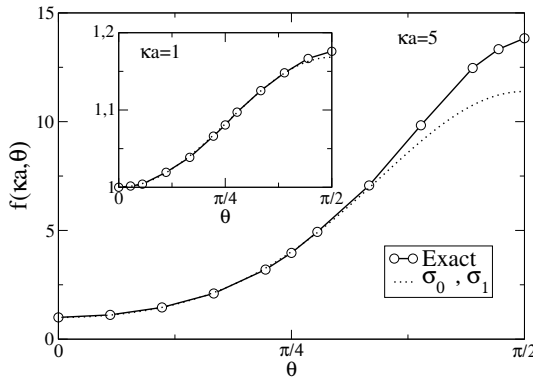


**Fig. 6.** Anisotropy function resulting from the two-parameter approximation (15) where  $\sigma_0$  and  $\sigma_1$  are determined from (17-18), compared to the exact result. The two above parameters are plotted in Figure 7. Here,  $\kappa a = 5$ , whereas  $\kappa a = 1$  in the inset.

From this expression, the anisotropy function may be computed and takes the form

$$f(\kappa a, \theta) = \frac{\sigma_0}{\sigma_0 + \sigma_1} \frac{2I_1(\kappa a \sin \theta)}{\kappa a \sin \theta} + \frac{\sigma_1}{\sigma_0 + \sigma_1} \frac{\sinh(\kappa a \sin \theta)}{\kappa a \sin \theta}. \quad (16)$$

In equations (13) and (16),  $I_0$  and  $I_1$  denote modified Bessel functions of the first kind, of order 0 and 1. Expressions (15) and (16) are not exact and there are several ways to choose the two parameters  $\sigma_0$  and  $\sigma_1$ , that will be determined by two constraints. The simplest possibility is to enforce  $\phi(0, 0) = \phi(a, 0) = \phi_0$ , but it turned that the choice (hereafter adopted)

$$\phi(0, 0) = \phi_0, \quad (17)$$

$$\langle \phi(\rho, 0) \rangle = \phi_0, \quad (18)$$

gave better results (the angular brackets denote average over the disc surface). In the limit  $\kappa \rightarrow 0$ , expressions (15)

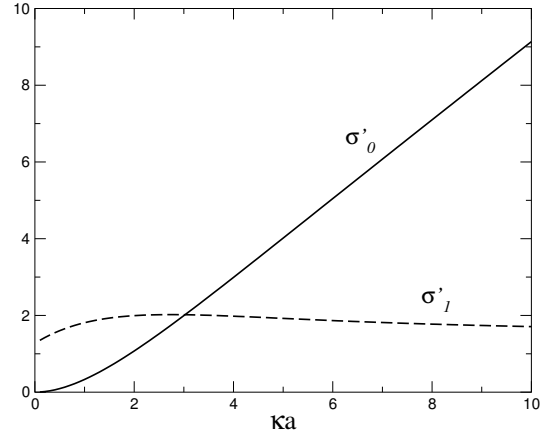


**Fig. 7.** Dimensionless charges  $\sigma'_{0,1} = 2\pi a \ell_B \sigma_{0,1} / (e\phi_0)$  following from (15) supplemented with equations (17-18), as a function of salinity conditions.

and (16) become exact (with  $\sigma_0 = 0$ ), and we expect that the comparison with exact results at finite  $\kappa$  will be all the better as  $\kappa a$  is low. It is indeed the case, but when  $\kappa a = 5$ , the approximation is still reasonable (see Figs. 5 and 6). By comparison with the exact solution Figure 6 shows that the anisotropy of the potential is correctly captured. The corresponding values of partial surface charges  $\sigma_0$  and  $\sigma_1$  are shown in Figure 7, where it may be observed that  $\sigma_0$  vanishes at low salt, as expected. The associated total charge  $Z$  is given by

$$Z = \frac{\pi a^2}{e} (\sigma_0 + \sigma_1) = \frac{a\phi_0}{2\ell_B} (\sigma'_0 + \sigma'_1), \quad (19)$$

where  $\sigma'_0$  and  $\sigma'_1$  are the quantities plotted in Figure 7. The charge  $Z$  is displayed in Figure 4, and compares favorably with its exact counterpart. In the above expression, however,  $\sigma_0$  and  $\sigma_1$  are functions of  $\kappa a$  with unknown analytical expression. As it is desirable to have an analytical formula, we propose the following argument: in the limit of large  $\kappa a$ , the disc essentially behaves as an infinite plane, from which we deduce  $Z\ell_B/a \sim \phi_0\kappa a/2$ . To estimate the next-order correction (constant term  $C$  in the expansion  $Z\ell_B/(a\phi_0) = (2\kappa a + C)/4$ ) we may take the limit  $\kappa a = 0$ , where the solution is given by (14), which imposes  $Z\ell_B/a = \phi_0/\pi$ . We, therefore, obtain

$$Z \frac{\ell_B}{a} \simeq \frac{\phi_0}{4} \left( 2\kappa a + \frac{4}{\pi} \right). \quad (20)$$

Anticipating that the relevant values of  $\phi_0$  are close to 4 (see Sects. 2 and 4), we have factorized the ratio  $\phi_0/4$  in the previous relation. The quality of approximation (20) is assessed in Figure 4, which shows a good agreement. On the other hand, extracting the correction factor  $C$  from the large  $\kappa a$  behaviour of the exact  $Z$  displayed in Figure 4 gives  $C \simeq 1.88$ , to be compared with  $C = 4/\pi \simeq 1.27$  in equation (20).

## 4 Numerical resolution of the non-linear Poisson-Boltzmann theory

In Section 3, we have obtained the solution of linearized PB theory with uniform potential boundary condition on the disc. From the discussion developed in Section 2, we expect the properties described (with  $\phi_0 = 4$ ) to characterize also the far field created by a highly charged disc, treated within non-linear PB theory. In the following, we critically test this scenario. We first present the numerical procedure used to solve the non-linear PB problem.

### 4.1 Green's function formalism and numerical method

Introducing explicitly the charge density  $q_d(\mathbf{r})$  borne by the disc, equation (1) is rewritten:

$$\nabla^2 \phi = \kappa^2 \sinh(\phi) + 4\pi\ell_B \frac{q_d(\mathbf{r})}{e}. \quad (21)$$

In the subsequent analysis, we will consider the case of a uniformly charged disc for which one has, in cylindrical coordinates

$$q_d(\mathbf{r}) = \sigma_{\text{bare}} \delta(z) \Theta(a - \rho), \quad (22)$$

where  $\Theta$  is the Heaviside step function and  $\delta$  the Dirac distribution. However, it is important to emphasize that the results that will be derived are more general, and hold irrespective of the precise PB boundary condition on the disc, provided the disc bare charge is high enough (phenomenon of effective potential saturation).

In view of a numerical resolution, it is convenient to rewrite (21) in the form

$$(\nabla^2 - \kappa_0^2)\phi = \kappa^2 \sinh(\phi) + 4\pi\ell_B q_d(\mathbf{r})/e - \kappa_0^2 \phi, \quad (23)$$

where  $\kappa_0$  is an arbitrary quantity that will be optimized in order to speed up the resulting procedure (see below). Introducing the Green's function

$$\mathcal{G}(\mathbf{r}, \mathbf{r}') = -\frac{e^{-\kappa_0|\mathbf{r}-\mathbf{r}'|}}{4\pi|\mathbf{r}-\mathbf{r}'|}, \quad (24)$$

solution of

$$(\nabla^2 - \kappa_0^2)\mathcal{G}(\mathbf{r}, \mathbf{r}') = \delta(\mathbf{r} - \mathbf{r}'), \quad (25)$$

we may recast (23) into

$$\phi(\mathbf{r}) = \int \mathcal{G}(\mathbf{r}, \mathbf{r}') \left[ \kappa^2 \sinh[\phi(\mathbf{r}')] + 4\pi\ell_B \frac{q_d(\mathbf{r}')}{e} - \kappa_0^2 \phi \right] d\mathbf{r}'. \quad (26)$$

The contribution arising from  $q_d$  may be computed analytically:

$$\frac{4\pi\ell_B}{e} \int \mathcal{G}(\mathbf{r}, \mathbf{r}') q_d(\mathbf{r}') d\mathbf{r}' = \frac{2Z\ell_B}{a} \int_0^\infty J_1(ak) J_0(k\rho) \frac{\exp(-|z|\sqrt{k^2 + \kappa^2})}{\sqrt{k^2 + \kappa^2}} dk \quad (27)$$

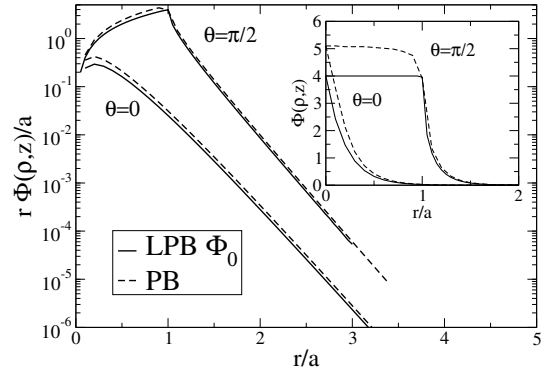


**Fig. 8.** Dashed line: electrostatic potential solution of PB equation (1) for a highly charged disc with uniform bare surface charge (Neumann-like boundary condition,  $Z_{\text{bare}} \ell_B/a = 60$ ). Here  $\kappa a = 5$ . The continuous line shows the solution of LPB theory with Dirichlet boundary condition  $\phi_0 = 4$  (see Sect. 3). The behaviour is shown along the two perpendicular directions  $\theta = 0$  and  $\theta = \pi/2$ . The main graph shows  $r\phi$  versus  $r/a = (\rho^2 + z^2)^{1/2}/a$  on a linear-log scale. The inset shows the previous potentials versus  $r$  on a linear scale.

and equation (26) is solved iteratively. Starting from the initial guess  $\phi_0 = 0$ , the right-hand side of (26), denoted  $\phi_0^{\text{out}}$ , is computed. This provides a new input potential  $\phi_1 = \alpha \phi_0^{\text{out}} + (1 - \alpha)\phi_0$ , which is itself inserted in the rhs of (26) to produce  $\phi_1^{\text{out}}$  etc. The mixing parameter  $\alpha$  is chosen in the range  $[10^{-2}; 10^{-1}]$ . Convergence  $\phi_n \simeq \phi_n^{\text{out}}$  is generally achieved for typically 50 to 200 iterations. The procedure may be accelerated starting not from  $\phi_0 = 0$  but from the solution of LPB theory (known in the present Neumann case, and given by Eq. (27)). In addition, it seems that the optimal choice for the numerical screening parameter  $\kappa_0$  is  $\kappa_0 \simeq \kappa$ . We have checked that the solutions found were independent of  $\kappa_0$  (as they should) by changing this parameter in the range  $[\kappa/5; 5\kappa]$ . The previous procedure bears similarities with the one used in reference [22], where a confined geometry was considered (whereas the situation is that of infinite dilution here).

### 4.2 Results

From the method sketched in Section 4.1, the numerical solution of the non-linear PB equation (1) may be obtained for arbitrary bare charges and salt content.

To test the constant potential picture put forward in Section 2 (which dwells on the fact that  $\kappa a$  is “large enough”) we show in Figure 8 the PB potential corresponding to a “large” bare charge. It appears that the PB and LPB potential are in excellent agreement except in the immediate vicinity of the disc, so that the constant effective potential prescription seems accurate.

From the PB potentials, we may also extract the effective charge  $Z_{\text{eff}}$  and anisotropy function  $f(\kappa a, \theta)$ , that convey a more complete information than a plot like that of Figure 8.  $Z_{\text{eff}}$  follows from the far-field behaviour along

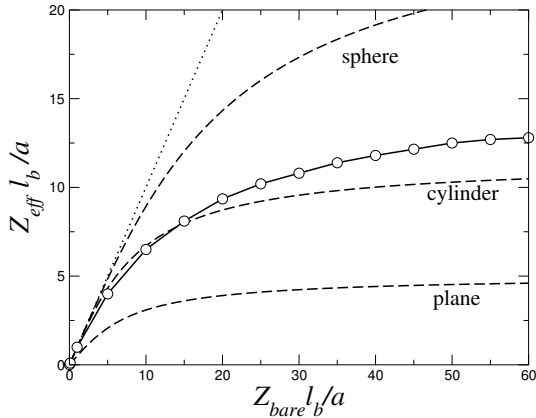


**Fig. 9.** Effective charge as a function of the bare one, for  $\kappa a = 5$ . The circles correspond to the PB solution, and the dotted line has slope one to show the regime of weak coupling, where  $Z_{\text{eff}} = Z_{\text{bare}}$ . The analytical expressions for a plane, a cylinder and a sphere have also been plotted (see labels).

the  $\theta = 0$  axis [23] (see Eq. (12)):

$$\phi(r, 0) \sim Z_{\text{eff}} \ell_B \frac{e^{-\kappa r}}{r}. \quad (28)$$

Once  $Z_{\text{eff}}$  is known,  $f$  is computed from equation (9). Expressions (12) and (28) are very similar, but the charges appearing have different status: in equation (12), the charge scales linearly with the  $\phi_0$  imposed within LPB, whereas in (28), the effective charge is a non-linear function of the platelet bare charge  $Z_{\text{bare}}$ . Note that in the present situation of infinite dilution, no procedure such as that proposed by Alexander and co-workers [24] is required:  $Z_{\text{eff}}$  has a simple and clear-cut meaning, which is not the case at finite density within a Wigner-Seitz cell, the situation investigated in [24].

For fixed  $\kappa a$ ,  $Z_{\text{eff}}$  is a function of the bare charge, see Figure 9, where the corresponding analytical predictions for planes, spheres and cylinders (of infinite length) have also been reported [17]. Not surprisingly, the behaviour is intermediate between that of infinite planes and spheres, and somehow resembles the results valid for charged cylinders. In addition,  $Z_{\text{eff}}$  reaches a saturation plateau when  $Z_{\text{bare}}$  becomes large [15] (see Fig. 9). This asymptotic plateau defines the effective charge at saturation  $Z_{\text{eff}}^{\text{sat}}$ , which is shown in Figure 10. This quantity is an increasing function of salt content (except for  $\kappa a < 0.5$ , see below), since an increase in salt density enhances the macroion/microion screening, which diminishes the amount of ‘‘counterion condensation’’ and consequently increases the effective charge [15]. Figure 10 shows that the constant potential prescription of Section 2 with  $\phi_0 = 4$  provides a satisfying description of highly charged platelets, as far as the (effective) charge is concerned. It also appears that the best linear interpolation reads

$$Z_{\text{eff}}^{\text{sat}} \ell_B / a \simeq 2\kappa a + 2.9, \quad (29)$$

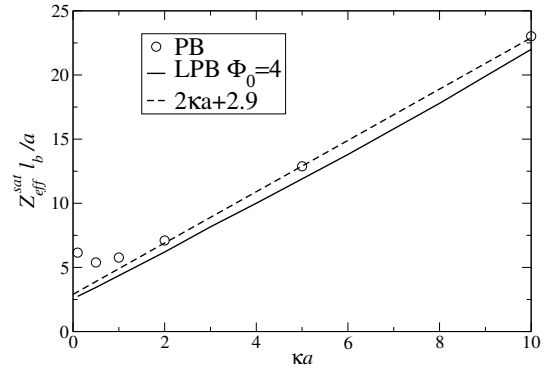


**Fig. 10.** Saturated effective charge  $Z_{\text{eff}}^{\text{sat}}$  as a function of salt (circles). The LPB charge  $Z$  is also shown for  $\phi_0 = 4$  (continuous line). The dashed line displays the empirical expression (29).

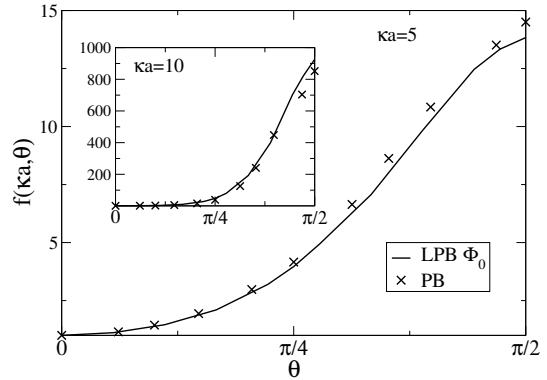


**Fig. 11.** Anisotropy function  $f(\kappa a, \theta)$  as a function of the azimuthal angle, for  $\kappa a = 5$ . The crosses correspond to the PB result with  $Z_{\text{bare}} \ell_B / a = 60$  (*i.e.* in the saturation regime) while the continuous curve shows the constant potential LPB result obtained in Section 3. Inset: same for  $\kappa a = 10$ .

which is rather close to approximation (20) with the choice  $\phi_0 = 4$ . It may be observed in Figure 10 that for low  $\kappa a$ , the effective charge increases when  $\kappa a$  decreases. This aspect will be discussed in Section 5.2.

Computation of anisotropy functions confirms the relevance of the constant effective potential picture (see the comparison proposed in Fig. 11). As shown in the inset, the very high values  $f \simeq 900$  predicted from the analysis of Section 3 are indeed found within non-linear PB. Note that the agreement reported in Figure 11 is only expected at high bare charges. For low bare charges,  $f(\kappa a, \theta)$  depends — at variance with its large bare charge counterpart — on the details on the boundary conditions chosen on the disc to solve PB. In the present situation (uniform surface charge),  $f$  may be computed analytically with the result [4]

$$f(\kappa a, \theta) = 2 \frac{I_1(\kappa a \sin \theta)}{\kappa a \sin \theta}. \quad (30)$$

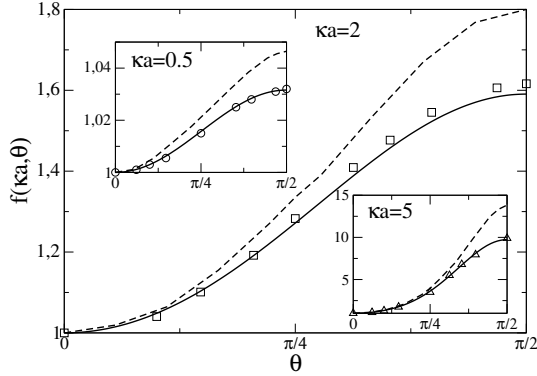


**Fig. 12.** Same as Figure 11, for a low bare charge  $Z_{\text{bare}} \ell_B/a = 10^{-2}$ . The circles, squares and triangles correspond to  $\kappa a = 0.5$ , 2 and 5, respectively. The prediction of equation (30) is shown by the continuous line. For the sake of comparison, we also plot with a dashed line the constant potential LPB result already displayed in Figure 11, which is relevant at high bare charges.

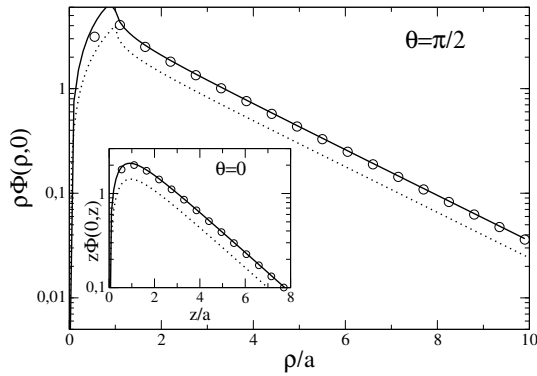


**Fig. 13.** Plot of the PB potential (continuous line) versus the distance from the disc center in the  $\theta = \pi/2$  direction (disc plane). Also displayed are the LPB results for  $\phi_0 = \phi_0^{\text{opt}} = 5.7$  (circles) and for  $\phi_0 = 4$  (dotted curve). Here,  $\kappa a = 0.5$  and  $Z_{\text{bare}} \ell_B/a = 15$  corresponding to the saturation plateau (the precise value of  $Z_{\text{bare}}$  is therefore irrelevant). The inset shows the same quantities along the disc normal.

This functional form is observed from our numerical data, for  $Z_{\text{bare}} \ell_B/a < 1$  (see Fig. 12). It turns out to differ much from that reported in Section 3 (shown with a dashed line in Fig. 12). We may also observe in Figure 12 that the “Neumann” expression (30) is lower than the Dirichlet one. The reason is the following:  $f$  is sensitive to the charges lying near the edge of the disc (see, *e.g.* Eqs. (10) and (13)). With Dirichlet boundary condition, the induced surface charge diverges (see App. B), at variance with the situation of a uniform surface charge, which therefore exhibits a less anisotropic potential. The Dirichlet and Neumann expressions, respectively, provide upper and lower bounds for the anisotropy function.

In spite of the good agreement shown in Figure 8, a slight difference may be observed between PB and LPB

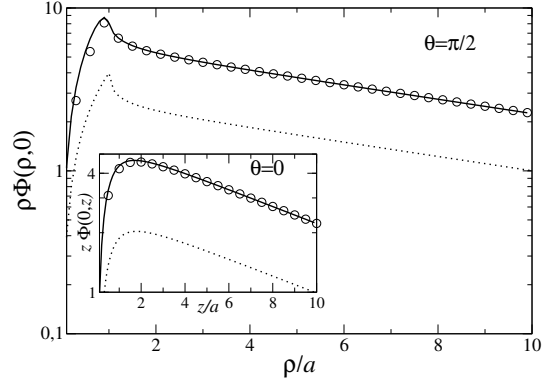


**Fig. 14.** Same as Figure 13 for  $\kappa a = 0.1$ , with  $\phi_0 = \phi_0^{\text{opt}} = 9.0$ .

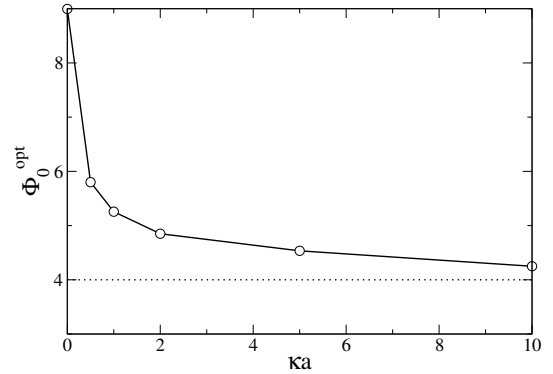


**Fig. 15.** Circles: values of the optimal surface potential  $\phi_0^{\text{opt}}$  to be imposed within LPB theory to produce the same far-field behaviour as a highly charged disc treated within PB (saturation limit). The dotted line indicates the high salt limiting behaviour  $\phi_0 = 4$ .

results. It may be concluded that a value  $\phi_0$  slightly above 4 may give a better agreement between non-linear and linear profiles. As mentioned at the end of Section 2, finite  $\kappa a$  corrections increase the value of the effective potential above 4 for spherical and rod-like macroions. Figures 13 and 14 show that a similar effect exists for discs: when the  $\phi_0$  of LPB approach is considered as an adjustable parameter, the agreement between PB and LPB (again for highly charged discs) becomes excellent even at relatively low values of  $\kappa a$ , such as  $\kappa a = 0.5$  or even  $\kappa a = 0.1$ . The salt dependence of the above optimal potential, denoted  $\phi_0^{\text{opt}}$ , is shown in Figure 15. One observes that  $\phi_0^{\text{opt}}$  is close to 4 for  $\kappa a > 5$ , but may take significantly different values at lower  $\kappa a$ . This leads to reconsider the plot of Figure 10 since the (relative) discrepancy PB/LPB may arise from discarding finite  $\kappa a$  effects (*i.e.* enforcing  $\phi_0 = 4$ ). Figure 16 compares PB saturated effective charge to its LPB counterpart, with  $\phi_0 = \phi_0^{\text{opt}}$ . Both quantities now agree very well. This latter comparison is a severe and successful test for the relevance of the constant potential prescription.

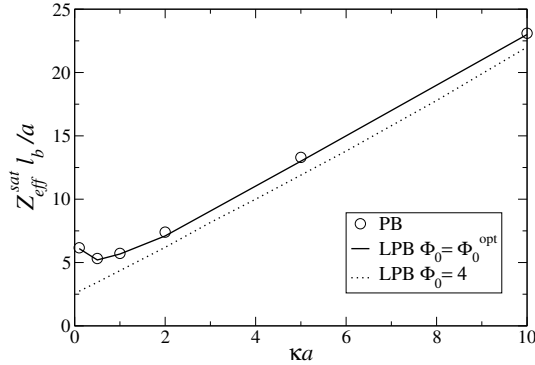


**Fig. 16.** Same as Figure 10 but with  $\phi_0 = \phi_0^{\text{opt}}$  (the latter quantity being plotted in Fig. 15) instead of  $\phi_0 = 4$ . For completeness, the results obtained with  $\phi_0 = 4$  are shown by the dotted line.

## 5 Discussion

### 5.1 Pair potential

From the properties of the one-body electrostatic potential  $\phi$  discussed previously, one may obtain the large-distance behaviour for the pair potential  $U_{12}$  in the situation of two discs (radii  $a_1$  and  $a_2$ ) in an electrolyte

$$U_{12} = Z_{\text{eff},1} Z_{\text{eff},2} \ell_B f(\kappa a_1, \theta_1) f(\kappa a_2, \theta_2) \frac{e^{-\kappa r}}{r}. \quad (31)$$

Here  $\theta_i$  is the angle between the normal to disc  $i$  and the center-to-center direction  $\mathbf{r}_{12}$  (with  $|\mathbf{r}_{12}| = r$ ). The validity of such an expression at intermediate or short distances (*i.e.*  $\kappa r$  of order 1) is unclear, since polarization effects of disc  $i$  on disc  $j$  should at least perturb the symmetry of the effective charge distribution, and hence alter the one-body expression for  $f$  plotted in Figure 11. We also note that the sub-leading terms in equation (31) that become more important as  $\kappa r$  decreases, involve a more complex dependence on relative orientations (with all Euler angles becoming relevant, contrary to the far-field case where only  $\theta_1$  and  $\theta_2$  matter).

We may conclude here that at fixed center-to-center distance  $r$ , the favored configuration is that where the discs are parallel and perpendicular to their center-to-center vector  $\mathbf{r}_{12}$ . The T-shape configuration is intermediate and the most repulsive one corresponds to coplanar discs (parallel to  $\mathbf{r}_{12}$ , as coins lying on a table). However, the situation changes if one fixes the closest distance  $\mathcal{D}$  between the two discs. Comparing the configuration  $\theta_1 = \theta_2 = \pi/2$ , where  $\mathcal{D} = r - a_1 - a_2$ , to that with  $\theta_1 = \theta_2 = 0$ , for which  $\mathcal{D} = r$ , requires to compare  $\mathcal{Q}$ , defined as

$$\mathcal{Q} = f\left(\kappa a_1, \frac{\pi}{2}\right) f\left(\kappa a_2, \frac{\pi}{2}\right) e^{-\kappa(a_1+a_2)}, \quad (32)$$

with 1. From the approximate expression (30), it appears that  $\mathcal{Q}$  is always smaller than 1. Instead of (30), a more

reliable expression for the anisotropy is provided by (16), which leads to the same conclusion. We, therefore, recover the intuitive result that the less repulsive configuration at fixed  $\mathcal{D}$  is for  $\theta_1 = \theta_2 = \pi/2$  (two coins on a table).

### 5.2 Behaviour at low $\kappa a$

In the present study, we have focused on the regime  $\kappa a > 1$  since according to the argument of Section 2, it corresponds to the situation where the effective potential may be predicted analytically. It appears that the Debye length acts as a local probe to reveal the anisotropy of the macroion under study. Hence, in the limit of small  $\kappa a$  where this probe cannot resolve the disc dimension, we found that the anisotropy disappears:  $f(\kappa a = 0, \theta) = 1, \forall \theta$ . We may then speculate that at small  $\kappa a$ , the precise form of the macroion becomes irrelevant so that we should recover the same results as for spheres [25]. From the analysis of Ramanathan [26], we may consequently expect in the saturation regime:

$$Z_{\text{eff}}^{\text{sat}} \frac{\ell_B}{a} \stackrel{\kappa a \ll 1}{\sim} -2 \ln(\kappa a) + 2 \ln[-\ln(\kappa a)] + 4 \ln 2. \quad (33)$$

Such an expression diverges for  $\kappa a \rightarrow 0$ , indicating that potential (or charge) renormalization ultimately becomes irrelevant. However, with the lowest value of  $\kappa a$  investigated in this work ( $\kappa a = 0.1$ ), we have measured  $Z_{\text{eff}}^{\text{sat}} \simeq 6.1 a/\ell_B$  (see Fig. 10), whereas equation (33) gives approximately a value 6.7. Whether this agreement is incidental or not is unclear. We also note that if the discs behave as spheres for very low  $\kappa a$ , their saturated effective potential should coincide with  $Z_{\text{eff}}^{\text{sat}} \ell_B/a$ . This is not the case for  $\kappa a = 0.1$ , where we measured  $\phi_0^{\text{opt}} \simeq 9$ . This may indicate what a salinity condition  $\kappa a = 1/10$  is not low enough to enter the “spherical” regime.

### 5.3 Validity of the PB approach

We now discuss the validity of the Poisson-Boltzmann theory underlying the present analysis. Such an approach neglects microionic correlations (be they of electrostatic or other origin, such as excluded volume) while macroion/microion electrostatic correlations are correctly incorporated. In the vicinity of the charged discs where the counterion density may become large, the neglected correlations are most important, and may invalidate PB theory if the disc bare charge is too large (say  $Z_{\text{bare}} > Z_{\text{bare}}^{\text{corr}}$ ). Since we have considered here the situation of high  $Z_{\text{bare}}$  to explore the PB saturation plateau, we need to justify the relevance of such a plateau. In other words, this amounts to elucidating the circumstances under which  $Z_{\text{sat}} < Z_{\text{bare}}^{\text{corr}}$ , since for  $Z_{\text{bare}} > Z_{\text{sat}}$ , one has, roughly speaking,  $Z_{\text{eff}} \simeq Z_{\text{sat}}$ .

For a salt-free system, Netz has considered the validity of PB theory in planar, cylindrical and spherical geometries [27]. Since no general result exists, we present here a simple argument concerning discs, which goes as

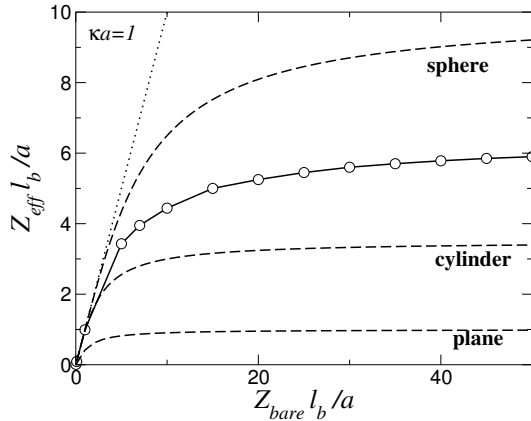


Fig. 17. Same as Figure 9 with  $\kappa a = 1$ .

follows (see [12] for the spherical case). Microionic correlations may be accounted for by the coupling parameter  $\Gamma = \ell_B/d$  where  $d$  is a typical distance between microions in the double layer. This distance is bounded from below by that, denoted  $d^*$ , where all  $Z$  monovalent counterions are artificially condensed onto the disc (as would happen in the low-temperature limit). It may be estimated writing that the typical surface per microion  $(d^*)^2$  on the disc is the mean value  $\pi a^2/Z$ . Hence,

$$\Gamma \simeq \sqrt{\ell_B^2 \sigma_{\text{bare}}} \simeq \sqrt{Z_{\text{bare}} \ell_B^2 / (\pi a^2)}. \quad (34)$$

For microions with valency  $z$ , one would obtain

$$\Gamma \simeq \sqrt{z^3 Z_{\text{bare}} \ell_B^2 / (\pi a^2)}. \quad (35)$$

For the sake of the argument, the factor  $\pi$  could be omitted. The important point here is that  $Z_{\text{bare}} \ell_B/a$  may be large, which corresponds to the saturation regime of PB theory, with still  $\Gamma < 1$ , which justifies the mean-field assumption underlying PB. With typical Laponite parameters [9] and monovalent microions, we have  $\Gamma \simeq 0.7$  for  $Z_{\text{bare}} \simeq 700$ , a reasonable value for the charge. In addition,  $Z_{\text{bare}} \ell_B/a \simeq 33$  which is well beyond the linear regime where effective and bare parameters coincide (see Fig. 9, or Fig. 17 corresponding to a lower salt concentration for which  $Z_{\text{bare}} \ell_B/a \simeq 33$  lies in the saturated region). We finally note that the intersection between the PB saturation regime and the consistency condition  $\Gamma < 1$  is all the larger as  $a/\ell_B$  is big [28]. But of course, when  $Z_{\text{bare}}$  strictly diverges,  $\Gamma$  exceeds a few units and PB breaks down. Finally, to be specific,  $Z_{\text{bare}}^{\text{corr}}$  would be defined as the value of  $Z_{\text{bare}}$  such that the coupling parameter  $\Gamma$  is of order unity. The case of Laponite seems somehow borderline, since  $Z_{\text{bare}}$  does not differ much from  $Z_{\text{bare}}^{\text{corr}}$  (on the order of a few thousands).

#### 5.4 The case of asymmetric electrolytes

Bearing in mind the classical rule that increasing the valency of microions decreases the range of validity of the

PB theory (see Eq. (35)), we may extend the previous results to 1 : 2 and 2 : 1 electrolytes. The key ingredient in the constant effective potential prescription is indeed the analytical solution of the planar (1D) PB equation. The latter problem has been solved by Gouy almost a century ago [29], and it turns out that the counterpart of the monovalent result  $\phi_0 = 4$  reads  $\phi_0 = 6$  for 2 : 1 electrolytes (*i.e.* monovalent counterions and divalent coions, or more precisely when the ratio of coion to counterion valency equals 2). In the reverse 1 : 2 situation, we have

$$\phi_0 = 6(2 - \sqrt{3}) \simeq 1.608. \quad (36)$$

The 1 : 2 effective potential is smaller than the 2 : 1 potential since screening by monovalent counterions is less efficient than with divalent ones (hence a higher effective potential, and a higher effective charge [30]).

By simply plugging the above expressions for  $\phi_0$  into the expressions derived in the previous sections for symmetric electrolytes, one may describe 1 : 2 and 2 : 1 situations as well. We finally note that the electrolyte asymmetry does not affect the anisotropy function  $f(\kappa a, \theta)$ : LPB equation takes the same form (modulo a change in the numerical value of  $\kappa$ ) and only  $\phi_0$  is affected.

#### 5.5 Comparison with existing results

In reference [4], we have addressed a similar issue as in the present paper. However, neither the LPB at constant potential nor the PB theory were solved. The anisotropy function has been estimated there from the Neumann LPB result with a uniform surface charge. This leads to expression (30), which has been shown in Figure 12 to be an underestimation of the Dirichlet result (and the agreement between PB and Eq. (30) is simply due to the low charge in Fig. 12, see Fig. 11).

Following similar lines, the saturated effective charge of discs have been estimated in [4] from the Neumann LPB solution. When the resulting dimensionless potential is equated to 4 on the disc center, we obtain [4]

$$Z_{\text{eff}}^{\text{sat}} = \frac{a}{\ell_B} \frac{2\kappa a}{1 - \exp(-\kappa a)}, \quad (37)$$

which is very close to  $2\kappa a$  as soon as  $\kappa a > 2$ . Such an expression only captures the leading-order behaviour (the planar limit), but misses the offset correction (2.9) as appears in equation (29).

## 6 Conclusion

We have presented in this paper a detailed comparison between the electrostatic potentials obtained within Poisson-Boltzmann (PB) and linearized PB (LPB) approximations, for a charged disc in an electrolyte. We have proposed a new and efficient semi-analytical method to solve the LPB problem at constant surface potential  $\phi_0$ . The procedure used is not restricted to the specific problem

considered here, and allows to solve more general situations of the form given by equation (A.3). On the other hand, the PB problem has been solved numerically following similar lines as in reference [22]. We have shown that the far-field potential created by a highly charged disc within PB is remarkably close to its LPB counterpart with a suitably chosen value of  $\phi_0$ , which therefore defines the effective potential of the charged discs. As expected from the argument put forward in Section 2, the latter quantity is close to 4 (meaning that the effective surface potential is close to  $4kT/e$ ) whenever  $\kappa a$  is larger than a few units, say  $\kappa a > 3$ . These results extend the conclusion of reference [15]. The argument of Section 2 should in fact apply for any charged macroion for which the curvature is smaller than the inverse Debye length  $\kappa$  of the surrounding electrolyte. Note also that in the limit of high bare charge, the details of the bare charge distribution onto the discs are irrelevant. In this respect, the results obtained here within PB with uniform surface charge are generic and would resist to charge modulation.

The scenario emerging is that due to non-linear screening phenomena, highly charged macroions may be considered as effective objects with a uniform surface potential and can be treated within a linear theory (provided short-distance features are irrelevant) which considerably simplifies the analysis and opens simulation routes. In addition, this potential is constant provided there is enough salt in the solution, in the sense that it no longer depends on physico-chemical parameters. Such a viewpoint not only predicts satisfactorily their effective charge, but also reproduces accurately the anisotropy of their potential. The latter property, embodied in the function  $f(\kappa a, \theta)$  is a key feature of screened electrostatic interactions and may have non-negligible —and hitherto largely unexplored— consequences. It is responsible for the rich-phase behaviour and orientational ordering of colloidal molecular crystals [31]. Its effects on the phase behaviour of clays, especially at moderately to high salt concentrations where large energy barriers  $f(\theta = \pi/2) - f(\theta = 0)$  are observed, will be the subject of future work.

The fact that highly charged asymmetric objects in solution of neutralizing counterions and salt behave effectively as objects with constant potential surfaces seems to be that despite the underlying fixed charged groups on the surface, the counterion cloud can freely adjust itself to “eliminate” unwanted lateral electric field by reorganizing itself as necessary, as perfect conductors do in Vacuum electrostatics. Since the focus so far as mostly been on isotropic objects, this point and the ensuing simplifications does not seem to have been appreciated.

The authors acknowledge fruitful discussions with J.J. Weis, B. Jancovici, F. van Wijland, M. Aubouy and H. Lekkerkerker. They would like to thank anonymous referees for valuable suggestions.

## Appendix A.

Mixed boundary value problems are rather frequent in electrostatics but also in diffusion and elasticity prob-

lems [33,32] (conduction of heat, diffusion of thermal neutrons, punch or crack problems etc.). They may be encountered in hydrodynamics as well [34]. They generally arise whenever a potential is prescribed over part of a boundary whereas its normal derivative is specified over the complementary part. The theory of dual integral equations turns out to be a powerful tool for such situations. In this appendix, we give more details about the problem of finding the solution  $A(k)$  to equations (7) and (8). To begin with, it is convenient to recast them in the form

$$\begin{cases} \int_0^\infty \frac{g(u)}{\sqrt{u^2 + (\kappa a)^2}} J_0(xu) du = 1, & \text{for } x < 1, \\ \int_0^\infty g(u) J_0(xu) du = 0, & \text{for } x > 1, \end{cases} \quad (\text{A.1})$$

where dimensionless quantities have been introduced:  $u = \kappa a$ ,  $x = \rho/a$  and  $g(u) = \sqrt{u^2 + (\kappa a)^2} A(u)/\Phi_0$ . Solutions of the previous equations for  $\kappa = 0$  (no salt case) have been derived by Titchmarsh [35]. The procedure, based on rephrasing the dual integral equations by means of some invertible linear operators gives the solution

$$A_{\kappa=0}(u) = \frac{2\Phi_0}{\pi} \frac{\sin u}{u} \quad (\text{A.2})$$

and the corresponding potential is that which leads to equation (14) for the charge. A generalization of Titchmarsh’s method has been proposed by Sneddon [36] for dual integral equations of the type

$$\begin{cases} \int_0^\infty u^{-2\alpha} (1 + \omega(u)) g(u) J_\nu(xu) du = 1, & \text{for } x < 1, \\ \int_0^\infty g(u) J_\nu(xu) du = 0, & \text{for } x > 1, \end{cases} \quad (\text{A.3})$$

where  $\omega$  is an arbitrary function. Equations (A.3) and (A.1) can be made equivalent by taking

$$\omega(u) = \frac{u}{\sqrt{u^2 + (\kappa a)^2}} - 1 \quad (\text{A.4})$$

with  $\alpha = 1/2$  and  $\nu = 0$  (for  $\omega(u) = 0$ , we recover the no salt case). The problem at hand —that fits into the general framework of [36]— may be reduced to that of solving a Fredholm equation of the second kind. Following Sneddon, we write equations (A.3) in the form:

$$\begin{aligned} S_{-\frac{1}{2},1}[(1 + \omega(u))g(u)/u, x] &= 2/x, & \text{for } x < 1, \\ S_{0,0}[g(u)/u, x] &= 0, & \text{for } x > 1, \end{aligned} \quad (\text{A.5})$$

where  $S_{\alpha,\beta}$  is the modified Hankel operator defined by

$$\begin{aligned} S_{\alpha,\beta}[\lambda(u), x] &\equiv S_{\alpha,\beta}\lambda(x) \\ &= 2^\beta x^{-\beta} \int_0^\infty u^{-\beta} \lambda(u) J_{2\alpha+\beta}(xu) du. \end{aligned}$$

We then introduce the function  $h$  through

$$g(u) = u S_{0,\frac{1}{2}}h(u). \quad (\text{A.6})$$

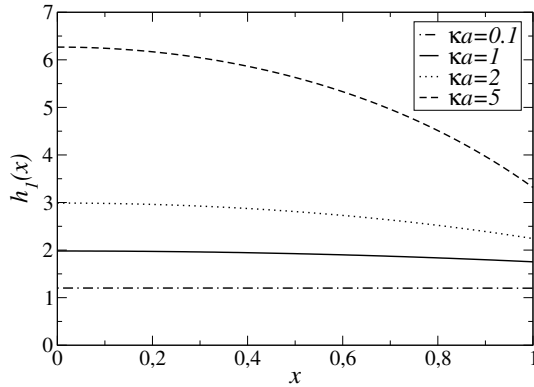


**Fig. 18.** Plots of  $h_1(x)$  (solution of the integral Eq. (A.7)) versus rescaled distance  $x$  for different values of  $\kappa a$ . For  $\kappa a = 0.1$ ,  $h_1$  is very close to its no salt limit  $2/\sqrt{\pi} \simeq 1.13$ .

This function  $h(u)$  is the central object in the present procedure. After some cumbersome algebra based on the properties of the modified Hankel operators (for details, see [36]), we find that the function  $h_2 = u h(u)$  defined on  $[1; \infty]$  vanishes while its counterpart  $h_1$  defined on  $[0; 1]$  is the solution of the following Fredholm equation of the second kind:

$$h_1(x) + \int_0^1 h_1(u) K(x, u) du = 2/\sqrt{\pi}. \quad (\text{A.7})$$

The kernel  $K(x, u)$  is defined in the whole  $xu$ -plane by

$$K(x, u) = \sqrt{\frac{\pi}{2}} \kappa a (I_1(\kappa a |x - u|) - L_1(\kappa a(x + u))) \quad (\text{A.8})$$

and  $I_1$  and  $L_1$  denote, respectively, the modified Bessel function and Struve function of the first kind, of order one. The weight function  $g(u)$  appearing in equation (A.1) is recovered by means of the integral

$$g(u) = \sqrt{u^2 + (\kappa a)^2} A(u) / \Phi_0 \quad (\text{A.9})$$

$$= \frac{u}{\sqrt{\pi}} \int_0^1 \cos(ut) h_1(t) dt. \quad (\text{A.10})$$

The potential finally follows from equation (6). The Fredholm equation (A.7) is solved numerically by an iterative procedure, starting by an constant initial guess for  $h_1$ .

In the limit  $\kappa = 0$ ,  $K(x, u) = 0$  so that, from equation (A.7),  $h_1 = 2/\sqrt{\pi}$ . The function  $g(u)$  in (A.10) follows immediately:  $g(u) = (2/\pi) \sin u$ , which is fully consistent with (A.2). Finally note that the functions  $h_1(x)$ , plotted in Figure 18 for different values of  $\kappa a$ , are related to the surface charge density of the disk  $\sigma(x)$  through the equation

$$\sigma(x) = \frac{h_1(x)}{\sqrt{\pi} \sqrt{1 - x^2}}. \quad (\text{A.11})$$

The function  $h_1$  can be well approximated by a quadratic polynomial. The corresponding charge  $\sigma(x)$  may then be used to compute analytically approximated effective

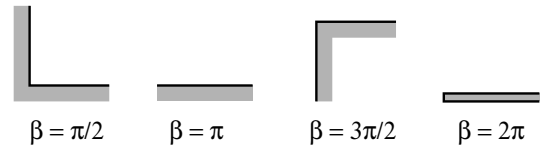


**Fig. 19.** The wedge geometry. The conductor is represented as the shadowed part and its boundaries by the thick line.

charges, anisotropy functions and weigh functions  $A(u)$ . This procedure is an alternative to the ansatz proposed in equation (15), the latter being more suited for an analytical treatment. We finally note that from equation (A.11) and the regular behaviour of  $h_1$  observed in Figure 18 for  $x \rightarrow 1$ , the surface charge diverges near the edge of the disc like  $(1 - x)^{-1/2}$ , see Appendix B.

## Appendix B.

We show here that the LPB surface charge distribution  $\sigma(\rho)$ —arising from the condition of constant surface potential on the disc—exhibits in an electrolyte the same edge effect as in vacuum, where it diverges as  $(a - \rho)^{-1/2}$  when  $\rho \rightarrow a^-$  [21].

We consider the more general problem of a wedged-shape conductor with angle  $\beta$  (see Fig. 19). The imposed potential is denoted  $\phi_0$ . Being interested in the behaviour near the sharp edge where the situation is of cylindrical symmetry, we introduce the cylindrical coordinates  $(r, \psi)$  in a plane perpendicular to the apex of the wedge. With rescaled distance  $\tilde{r} = \kappa r$ , we look for solutions of LPB equation (2):

$$\tilde{r} \frac{\partial}{\partial \tilde{r}} \left( \tilde{r} \frac{\partial \phi}{\partial \tilde{r}} \right) + \frac{\partial^2 \phi}{\partial \psi^2} = \tilde{r}^2 \phi, \quad (\text{B.1})$$

in a form with separated variables:

$$\phi(\tilde{r}, \psi) = R(\tilde{r}) \Psi(\psi). \quad (\text{B.2})$$

With the boundary condition  $\phi(\tilde{r}, \psi = 0) = \phi(\tilde{r}, \psi = \beta) = \phi_0$  for all  $\tilde{r}$  in the vicinity of the wedge (*i.e.*  $\tilde{r}$  close to 0), the solution reads

$$R(\tilde{r}) = A_\nu I_\nu(\tilde{r}), \quad (\text{B.3})$$

$$\Psi(\psi) = \alpha_\nu \sin(\nu \psi). \quad (\text{B.4})$$

Here,  $\nu = n\pi/\beta$ , where  $n \in \mathbb{N}$ ;  $A_\nu$  and  $\alpha_\nu$  are arbitrary constants. In the vicinity of the wedge, the potential therefore takes the form

$$\phi(\tilde{r}, \psi) = \phi_0 + \sum_{n=1}^{\infty} A_n \sin\left(\frac{n\pi\psi}{\beta}\right) I_{n\pi/\beta}(\tilde{r}). \quad (\text{B.5})$$

The dominant term when  $\tilde{r} \rightarrow 0$  corresponds to  $n = 1$ , and scales like  $\tilde{r}^{\pi/\beta}$ . The associated surface charge behaves like  $\sigma(\tilde{r}) \propto \tilde{r}^{\pi/\beta - 1}$ , hence like  $\tilde{r}^{-1/2}$  near the edge of a disc ( $\beta = 2\pi$ ). This result has been used to choose the functional form (15).

## References

1. A. Mourchid, A. Delville, J. Lambard, E. Lécolier, P. Levitz, *Langmuir* **11**, 1942 (1995); A. Mourchid, E. Lécolier, H. van Damme, P. Levitz, *Langmuir* **14**, 4718 (1998).
2. D. Bonn, H. Kellay, H. Tanaka, G. Wegdam, J. Meunier, *Langmuir* **15**, 7534 (1999).
3. T. Nicolai, S. Coccoard, *J. Colloid Interface Sci.* **244**, 51 (2001).
4. E. Trizac, L. Bocquet, R. Agra, J.-J. Weis, M. Aubouy, *J. Phys. Condens. Matter* **14**, 9339 (2002).
5. F. Cousin, V. Cabuil, P. Levitz, *Langmuir* **18**, 1466 (2002).
6. L.J. Michot, J. Ghanbaja, V. Tirtaatmadja, P.J. Scales, *Langmuir* **17**, 2100 (2001).
7. D. Rowan, J.-P. Hansen, *Langmuir* **18**, 2063 (2002).
8. D. van der Beek, H.N.W. Lekkerkerker, *Europhys. Lett.* **61**, 702 (2003).
9. These colloidal discs bear a negative bare charge. They have a radius of approximately 15 nm and a thickness smaller than 1 nm, see, *e.g.*, Laponite technical report, Southern Clay Products Inc., Laporte plc. The results reported here correspond to a positive bare charge. They immediately transpose to the Laponite case by a change of sign.
10. L. Belloni, *Colloids Surf. A* **140**, 227 (1998); *J. Phys. Condens. Matter* **12**, R549 (2000).
11. J.-P. Hansen, H. Löwen, *Annu. Rev. Phys. Chem.* **51**, 209 (2000).
12. Y. Levin, *Rep. Prog. Phys.* **65**, 1577 (2002).
13. F. Oosawa, *Polyelectrolytes* (Dekker, New York, 1971).
14. D. Chapot, L. Bocquet, E. Trizac, *J. Chem. Phys.* **120**, 3969 (2004).
15. E. Trizac, L. Bocquet, M. Aubouy, *Phys. Rev. Lett.* **89**, 248301 (2002); L. Bocquet, E. Trizac, M. Aubouy, *J. Chem. Phys.* **117**, 8138 (2002).
16. D. Andelman in *Membranes, their Structure and Conformation*, edited by R. Lipowsky, E. Sackmann (Elsevier, Amsterdam, 1996).
17. M. Aubouy, E. Trizac, L. Bocquet, *J. Phys. A* **36**, 5835 (2003).
18. From equation (5), highly charged means in practice  $\sigma \gg \kappa\epsilon/\ell_B$ .
19. J.D. Jackson, *Classical Electrodynamics* (John Wiley & Sons, New York, 1975).
20. E. Trizac, J.P. Hansen, *Phys. Rev. E* **56**, 3137 (1997).
21. L.D. Landau, E.M. Lifschitz, *Electrodynamics of Continuous Media* (Pergamon Press, Oxford, 1984).
22. R.J.F. Leote de Carvalho, E. Trizac, J.-P. Hansen, *Europhys. Lett.* **43**, 369 (1998).
23. The existence of a given direction along which the effective charge may be directly measured is a specific feature of macroions with vanishing internal volume. In general, as happens for a disc of finite thickness, the anisotropy function  $f$  differs from unity in all directions. It is consequently more difficult—and to some extent arbitrary—to disentangle effective charge effects from those due to anisotropy.
24. S. Alexander, P.M. Chaikin, P. Grant, G.J. Morales, P. Pincus, *J. Chem. Phys.* **80**, 5776 (1984).
25. We are interested here again in the far-field behaviour. For  $\kappa = 0$  (no electrolyte), a disc and a sphere behave identically, as a usual monopole.
26. G.V. Ramanathan, *J. Chem. Phys.* **88**, 3887 (1988).
27. R.R. Netz, *Eur. Phys. J. E* **5**, 557 (2001); **13**, 43 (2004).
28. A similar conclusion is reached in R.D. Groot, *J. Chem. Phys.* **95**, 9191 (1991).
29. G.L. Gouy, *J. Phys.* **9**, 457 (1910).
30. G. Téllez, E. Trizac, *Phys. Rev. E* **70**, 011404 (2004).
31. R. Agra, F. van Wijland, E. Trizac, *Phys. Rev. Lett.* **93**, 018304 (2004).
32. W.D. Collins, *Mathematika* **6**, 120 (1959).
33. I.N. Sneddon, M. Lowengrub, *Crack Problems in the Classical Theory of Elasticity* (John Wiley, New York, 1969).
34. H. Lamb, *Hydrodynamics*, 6th ed. (Cambridge University Press, 1932).
35. E.C. Titchmarsh, *Introduction to the Theory of Fourier Integrals*, 2nd ed. (Clarendon Press, Oxford, 1948).
36. I.N. Sneddon, *Mixed Boundary Value Problems in Potential Theory* (North Holland, 1966).